Article

Cell Reports

Parallel In Vivo and In Vitro Melanoma RNAi Dropout Screens Reveal Synthetic Lethality between Hypoxia and DNA Damage Response Inhibition

Graphical Abstract

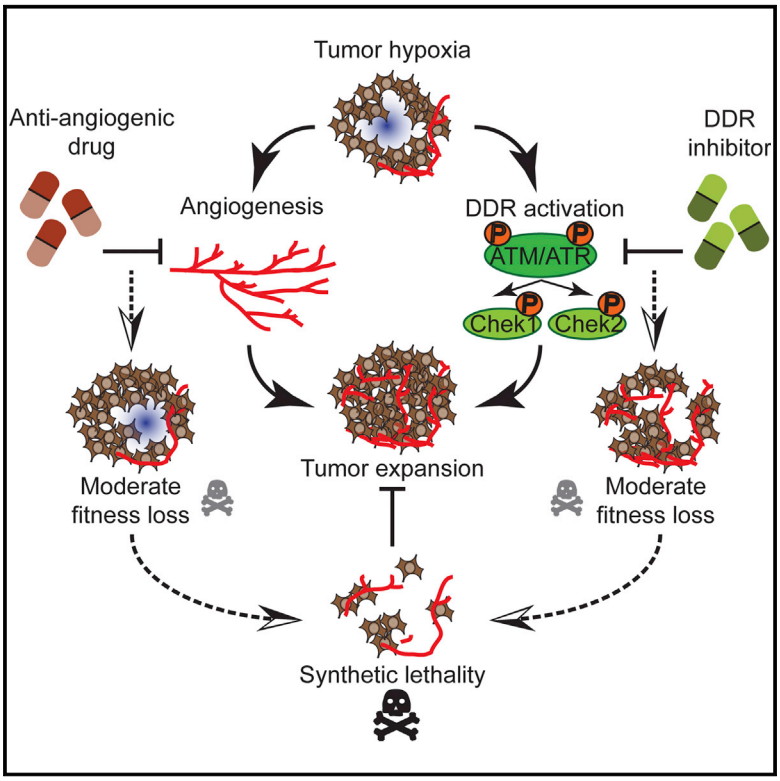

Authors

Patricia A. Possik, Judith Müller, ..., Ton N. Schumacher, Daniel S. Peeper

Correspondence

d.peeper@nki.nl

In Brief

Specific parameters lacking in vitro, but present in vivo, influence tumor behavior and therapeutic dependencies. Possik et al. now perform parallel in vitro and in vivo negative-selection screens and uncover a critical requirement for DNA damage response kinases in expanding tumors, a liability that could be exploited pharmacologically.

Highlights

Parallel in vitro and in vivo RNAi screens identify specific tumor dependencies

DDR kinases are activated following hypoxia during tumor expansion

Tumor growth is dependent on DDR kinase activity

A "druggable" synthetic lethal relationship exists between DDR inhibition and hypoxia

Accession Numbers

GSE61826

Possik et al., 2014, Cell Reports 9, 1375–1386
November 20, 2014 ©2014 The Authors
http://dx.doi.org/10.1016/j.celrep.2014.10.024

Cell Reports
Article

Parallel In Vivo and In Vitro Melanoma RNAi Dropout Screens Reveal Synthetic Lethality between Hypoxia and DNA Damage Response Inhibition

Patricia A. Possik,[1] Judith Müller,[1] Carmen Gerlach,[2,5] Juliana C.N. Kenski,[1] Xinyao Huang,[1] Aida Shahrabi,[1] Oscar Krijgsman,[1] Ji-Ying Song,[3] Marjon A. Smit,[1,6] Bram Gerritsen,[4,7] Cor Lieftink,[4] Kristel Kemper,[1] Magali Michaut,[4] Roderick L. Beijersbergen,[4] Lodewyk Wessels,[4] Ton N. Schumacher,[2] and Daniel S. Peeper[1,*]
[1]Division of Molecular Oncology, The Netherlands Cancer Institute, 1066 CX Amsterdam, the Netherlands
[2]Division of Immunology, The Netherlands Cancer Institute, 1066 CX Amsterdam, the Netherlands
[3]Division of Experimental Animal Pathology, The Netherlands Cancer Institute, 1066 CX Amsterdam, the Netherlands
[4]Division of Molecular Carcinogenesis, The Netherlands Cancer Institute, 1066 CX Amsterdam, the Netherlands
[5]Present address: Department of Microbiology and Immunobiology, Harvard Medical School, Boston, MA 02115, USA
[6]Present address: Department of Hematology, VU University Medical Center, Cancer Center, 1081 HY Amsterdam, the Netherlands
[7]Present address: Department of Biology, Utrecht University, 3584 CH Utrecht, the Netherlands
*Correspondence: d.peeper@nki.nl
http://dx.doi.org/10.1016/j.celrep.2014.10.024

SUMMARY

To identify factors preferentially necessary for driving tumor expansion, we performed parallel in vitro and in vivo negative-selection short hairpin RNA (shRNA) screens. Melanoma cells harboring shRNAs targeting several DNA damage response (DDR) kinases had a greater selective disadvantage in vivo than in vitro, indicating an essential contribution of these factors during tumor expansion. In growing tumors, DDR kinases were activated following hypoxia. Correspondingly, depletion or pharmacologic inhibition of DDR kinases was toxic to melanoma cells, including those that were resistant to BRAF inhibitor, and this could be enhanced by angiogenesis blockade. These results reveal that hypoxia sensitizes melanomas to targeted inhibition of the DDR and illustrate the utility of in vivo shRNA dropout screens for the identification of pharmacologically tractable targets.

INTRODUCTION

It is well established that many cancers are ''addicted'' to certain altered genes, a vulnerability that can be exploited therapeutically. Equally interesting is the premise that tumors express genes that are not mutated, but to which they are addicted nonetheless. Owing to several stress factors, including adaptation to their microenvironment, cancer cells are under continuous selective pressure to survive. This requires substantial deregulation of unmutated signaling factors, and also this phenomenon can create tumor-specific dependencies. Targeting this ''non-oncogene addiction'' therefore represents a complementary tactic to exploiting oncogene addiction (Luo et al., 2009). This strategy builds on the concept of ''synthetic lethality,'' which is based on the principle that a single (genetic) perturbation is compatible with cell viability, but a second concomitant alteration is lethal (Kaelin, 2005). It was not until the completion of the human genome sequence as well as the availability of genome-wide RNAi that the concept of synthetic lethality could be translated to experimental mammalian systems.

Several examples illustrate the feasibility of drug effectiveness and selectivity in the context of non-oncogene addiction and synthetic lethality. For example, *BRCA1/2*-deficient breast cancers are highly sensitive to inhibitors targeting PARP (Farmer et al., 2005; Sharma and Settleman, 2010). Similarly, in *BRAF* mutant melanomas, there is a strict requirement for MEK (Flaherty et al., 2012; Kaelin, 2004; Sawyers, 2005; Solit et al., 2006) and ERK (Chapman et al., 2011; Hauschild et al., 2012; Morris et al., 2013). In addition, melanoma cells are highly dependent on pyruvate dehydrogenase kinase (PDK1), the gatekeeper enzyme linking glycolysis to the citric acid cycle (Kaplon et al., 2013). These examples suggest that also the ''non-oncogenome'' ought to be exploited for drug-target discovery.

Both the limited number of clinically approved targeted drugs available and the challenging problem of common drug resistance, which can be highly pleiotropic (Jang and Atkins, 2013), underscore the need to identify novel factors amenable to targeted interference. Systematic gene silencing by RNAi libraries in cancer cells has proven to reveal such unforeseen cellular dependencies. However, because these experiments are commonly performed in vitro, they ignore the effects of in vivo parameters on both tumor progression and drug response. The complex and harsh conditions resulting from tumor expansion such as nutrient deprivation, limited oxygen availability, and the generation of reactive oxygen species (Lee and Herlyn, 2007) are difficult to mimic in cell culture. It is likely, therefore, that the functional mining of ''druggable'' targets has been far from complete and that, particularly under in vivo conditions, additional factors that are essential for tumor expansion can be

unmasked. Therefore, we set out to perform parallel in vivo and in vitro negative-selection short hairpin RNA (shRNA) screens for genes that preferentially contribute to tumor cell proliferation and survival in vivo.

RESULTS

Xenografted Human Melanomas Accommodate Large Library Complexities with Minimum Random Loss

A rate-limiting requirement for a negative-selection shRNA screen in tumors is the prevention of random loss of cells, and thereby shRNAs, which is seen when only a fraction of the cells contribute to the expanding tumor mass. In most human tumor types, only specific subpopulations of cells are endowed with tumorigenic potential when transplanted into immune-compromised mice (Shackleton et al., 2009). Also for melanomas, the presence of tumor-initiating cells has been reported (Boiko et al., 2010; Roesch et al., 2010; Schatton et al., 2008). However, specific modifications in the xenotransplantation methods strongly increase the efficiency of melanoma formation (Quintana et al., 2008, 2010). In particular, when tumor cells are embedded in Matrigel and inoculated into severely immune-compromised NOD/SCID IL2Rγ^{null} (NSG) mice human melanomas develop faster and more efficiently, even when inoculated as single cells. Because under these conditions most melanoma cells have tumor-forming potential, we selected this tumor type and mouse model for the screens outlined below.

To investigate whether such conditions are compatible with negative-selection screening of high-complexity shRNA libraries, we first performed a proof-of-principle experiment using a GFP-tagged library comprising 2,600 barcodes (noncoding semirandom DNA sequences), which do not affect cellular fitness. This library has been employed successfully to dissect T cell lineage relationships previously (Gerlach et al., 2013; Schepers et al., 2008). Our feasibility experiment was based on the premise that similar recoveries of the barcodes from independent tumors would indicate that a sufficient number of cells participate in tumor establishment. The barcode library was introduced into melanoma cells by retroviral transduction using a low multiplicity of infection (MOI) to ensure that each cell received one barcode copy only. GFP-positive cells were sorted and inoculated subcutaneously (s.c.) into two NSG mice (Figure 1A). We removed the tumors from the mice when they reached a measurable size and subsequently analyzed the distribution of barcodes.

Genomic DNA isolated from each tumor was divided into two half-samples, and a "self-self" test showed that the ratio between barcodes detected in each sample was close to one for both tumors (Figure S1), indicating that the prevalence of individual genetic tags could be reproducibly quantified. This result also predicted that statistically significant outliers in self-nonself comparisons (in an shRNA screen) would be real. More importantly, comparison of the two biological replicates showed a remarkably large overlap of barcodes (Figure 1B). This indicated that in independent transplanted melanomas, a sufficient number of cells contribute to tumor establishment and confirmed the feasibility of a large-scale dropout screen in vivo.

Differential shRNA Depletion in Cultured Cells and Expanding Tumors

To perform parallel in vitro and in vivo screens, we assembled an shRNA library targeting ~500 human kinases (and related factors), with approximately five shRNAs per gene. The aim was to detect shRNAs that are selected against in vivo, but not or to a lesser extent in vitro, to identify pharmacologically tractable factors critically contributing to tumor expansion. Human melanoma cells were transduced with four lentiviral pools, together encoding the shRNA kinome library, and subsequently pharmacologically selected for successful integration and expression (Figure 1C). Two days postinfection, two independent reference samples were collected to make an inventory of the shRNAs present at the start of the screens. The remaining cells were split in two, and the first group was resuspended in Matrigel and immediately transplanted s.c. into six NSG mice. Because we aimed to identify shRNAs preferentially depleted in expanding tumors relative to an in vitro setting, we maintained the second group of cells in parallel in culture. This was done in six independent cell culture plates and for approximately the same period that the tumors were expanding in mice. Once the tumors had reached 60–100 mm^3, they were removed from the mice and genomic DNA was extracted, as well as from the cultured tumor cells. We used PCR amplification of the shRNAs followed by deep sequencing for the recovery and quantification of shRNAs present in each sample.

To select genuine "dropouts," that is, shRNAs that were depleted during either in vitro propagation or during tumor expansion in vivo, we performed a strict quality-control analysis on the sequencing data. The number of shRNAs detected in each sample demonstrated that the library complexity was very well maintained in all samples in vitro and in vivo: approximately 93% of the shRNAs that were detected in the reference samples were reproducibly observed in cultured cells, while 85% of the shRNAs originally present were retrieved from the tumors (Figure 1D). Similar to what was seen for the barcode experiment, we observed a high correlation between independent biological replicates (Figure 1E). Unsupervised analysis showed clustering of all samples within each biological group, indicating that random changes were minor relative to the difference between in vitro and in vivo tumor growth (Figure 1F). Corroborating the results from the barcode screen, these data predict that the likelihood of selecting false-positive hits was minimal.

Identification and Validation of In Vivo shRNA Dropout Hits

To call hits, that is, to identify genes with a significant role in vivo, we applied several criteria. First, we selected genes for which at least two independent shRNAs were significantly depleted in tumors compared to both the references and the cultured cells (Figures 2A, 2B, and S2A). Second, we filtered out genes for which two or more shRNAs were depleted from cultured cells compared to the references (Figure S2B). For example, one gene that failed to score as a hit based on these stringent criteria is *BRAF*. The mutant form of *BRAF* acts as the driver oncogene in melanoma (Davies et al., 2002), and its depletion induces cell death both in vitro and in vivo (Hingorani et al., 2003; Tsai et al., 2008). Indeed, although we observed loss of *BRAF*-targeting

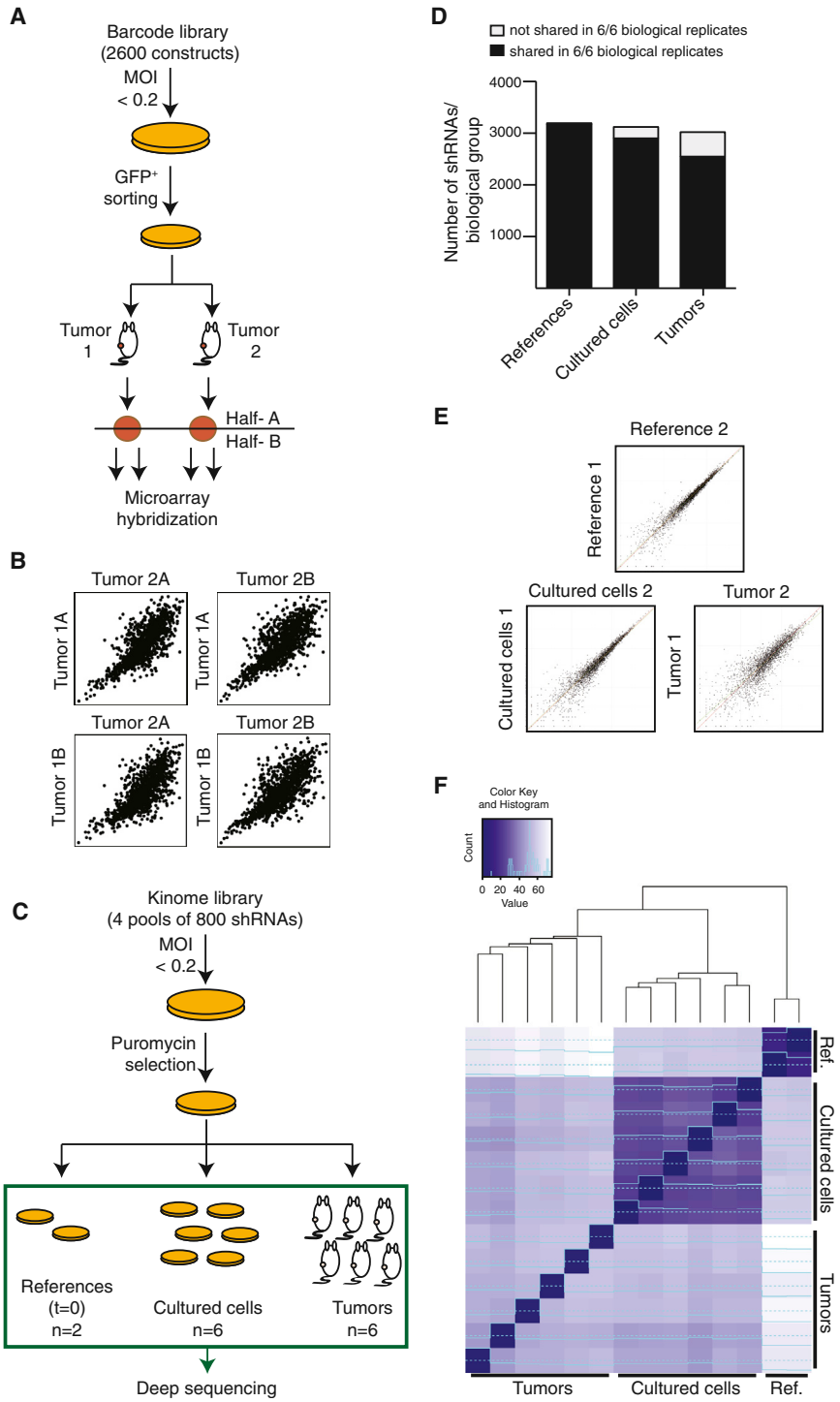

Figure 1. Parallel In Vitro and In Vivo Screens Show Differential shRNA Depletion

(A) Scheme of the barcode screen. 888mel human melanoma cells were transduced with a retroviral GFP-tagged barcode library (MOI < 0.2). After fluorescence-activated cell sorting, cells were transplanted s.c. into two NSG mice. Genomic DNA from each tumor was divided into two half-samples. Barcodes from each were amplified, labeled with Cy3 (A) and Cy5 (B), and hybridized to a microarray platform containing the entire library. See also Figure S1.

(B) Comparison of barcode representation in two independent tumors. Each dot represents a unique barcode. The y and x axes show the $\log_{10}$ fluorescence intensity as a measure of barcode representation in tumor 1 (half-samples A and B) compared to tumor 2 (half-samples A and B).

(C) Scheme of the in vivo and in vitro screens. The lentiviral kinome library was divided into four pools and used to transduce 888mel cells (MOI < 0.2). After puromycin selection, two reference samples were collected. The remaining cells were split and either transplanted s.c. into six NSG mice (one flank each) or plated into six independent plates for in vitro culturing. Thirteen days later, genomic DNA was isolated and deep sequencing was used to quantify the shRNAs present in each sample.

(D) Library quantification. Each bar shows the average number of different shRNAs per biological group of samples. References serve as a control. From 3,195 shRNAs detected in the references, 3,121 were identified in cultured cells and 3,020 in tumors. Dark areas of the bars represent shRNAs that were shared between all six biological replicates, which account for 93% in vitro and 84.3% in vivo.

(E) Comparison of biological replicates. Each dot represents a unique shRNA. The x and y axes show the $\log_{10}$ abundance of shRNAs. A representative example of two biological replicates is shown per group. Average-adjusted R^2 values are 0.94, 0.89, and 0.76 for references, cultured cells, and tumor correlations, respectively.

(F) Global view of biological similarity as illustrated by the Euclidean distance heatmap, indicating the degree of similarity between samples (see color key). Light blue bars plotted inside color key represent counts of individual heatmap units (individual correlations) with the assigned Euclidean distance value.

shRNAs, this occurred to similar extents in vitro and in vivo (Figure S3A); hence, *BRAF* failed to classify as a preferential in vivo target. Seven genes did meet our criteria: they were depleted by two or more shRNAs to a significantly greater extent in vivo than in vitro (Figure 2A). The identification in the screen of *FRAP1*, encoding mTOR, was reassuring because of the established role it plays in melanoma (Karbowniczek et al., 2008).

Critical Role for DNA Damage Response Factors during Melanoma Expansion

A key advantage of large-scale shRNA screening, in addition to its unbiased nature, is the possibility of identifying multiple pathway components rather than single factors. We noted that two out of the seven screen hits were key kinases involved in the DNA damage response (DDR), ATM and Chek1, while Chek2 scored with

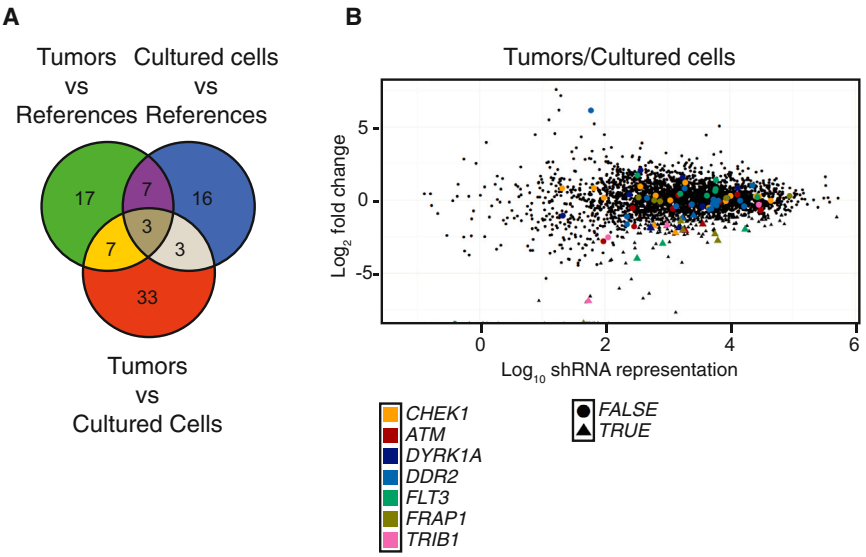

Figure 2. Identification of In Vivo shRNA Dropout Hits

(A) Venn diagram illustrating the overlap of the three independent analyses. The seven genes in the intersection of tumors versus cultured cells and tumors versus references were selected as hits with a preferential effect in vivo.

(B) DESeq analysis comparing tumors versus cultured cells. The x axis shows the $\log_{10}$ average shRNA abundance across all samples. The y axis shows the $\log_2$ fold change of tumors versus cultured cells. Symbols distinguish shRNAs that are significantly depleted in tumors compared to cultured cells (triangles, true) from the unchanged or nonsignificant ones (circles, false). Each color represents a gene selected as a hit. See also Figure S2.

one shRNA. Because it is an established substrate of ATM, we included Chek2 in the subsequent validation. In the screen, shRNAs targeting these three genes were more strongly selected against in vivo than in vitro, resulting in some cases in their complete loss in tumor xenografts (Figures S3B–S3D).

To validate these results, we stably knocked down these three genes one by one, inoculated the melanoma cells into NSG mice, and monitored tumor growth. Silencing of *CHEK1*, *CHEK2*, or *ATM*, each with independent shRNAs, profoundly delayed tumor growth (Figures 3A–3C). *CHEK1* shRNA #2 and *CHEK2* shRNAs #1 and #2 particularly showed minimal effect on cell viability in vitro but caused strong tumor inhibition in vivo (Figures 3A–3C, inserts). We did not observe major differences in the expression levels of the proliferation marker PCNA in cell cultures versus tumor cells that grew in mice (Figure S3E), suggesting that this cannot account for the observed differential sensitivity to *CHEK1*, *CHEK2*, or *ATM* depletion. The average weights of sh*CHEK1*, sh*CHEK2*, and sh*ATM* tumors extracted at the endpoint of the experiment were significantly lower than those of control tumors (Figures S3F–S3H). Notably, whereas an efficient knockdown of all these genes was confirmed before injection, tumors that eventually grew out had restored their expression, consistent with the idea that silencing of any of these DDR genes is incompatible with melanoma outgrowth in vivo (Figures 3D–3F). Taken together, these observations indicate that three established DDR kinases individually have essential roles in driving melanoma expansion.

The DNA Damage Response Pathway Is Activated during Tumor Expansion In Vivo

We next investigated why deprivation of DDR factors confers a strong selective disadvantage onto expanding melanomas. We hypothesized that the DDR may be induced as a function of tumor expansion. Indeed, six out of six melanomas established in mice displayed increased phosphorylation of ATM, Chek1, and Chek2 relative to cells cultured in vitro (Figure 4A). When monitoring the dynamics of this phenomenon in an independent experiment, we found no evidence for activation of the DDR pathway in the first week after transplantation (Figure 4B). This result argues that the DDR was not induced artificially because of the mere transfer of the cells from cell culture dishes into animals. In contrast, we consistently observed induction of these DDR factors from 2 weeks post-inoculation onward, until the time that tumors reached 500 mm^3. The activation of these DDR kinases coincided with the phosphorylation of an array of ATM/ATR substrates. The same pattern on the levels of DDR factors was observed when transplanting a different cell line, ruling out cell-type-specific effects (Figure S4A).

DDR Signaling Is Induced by Hypoxia and HIF1α Signaling In Vitro and Colocalizes with Hypoxic Areas of Tumors In Vivo

DDR signaling can be activated in response to different kinds of environmental and endogenous stress signals. In order for tumors to expand, a key obstacle to overcome is to proliferate and survive under suboptimal conditions. This includes the lack of proper vasculature, necessary for transporting nutrients and oxygen (Pouysségur et al., 2006). In fact, hypoxia can activate ATM and ATR checkpoints, and hypoxic tumor cells display defective DNA repair, increased mutation rates, and chromosomal instability (Bencokova et al., 2009; Hammond et al., 2007; Olcina et al., 2010). Expanding tumors had abundant levels of Hypoxia-Inducible Transcription Factor 1α (HIF1α), the master transcription factor controlling cellular adaptation to low oxygen levels (Figure 5A). Following its stabilization, DDR signaling was induced. That this link between hypoxia and DDR may be causal was further suggested by the strong increase in phosphorylation of both ATM and Chek2, which followed the induction of HIF1α by hypoxia in vitro (Figure 5B).

Under hypoxic conditions, HIF1α becomes stabilized, allowing for dimerization with HIF1β and inducing an arsenal of genes to help cells cope with harsh microenvironmental conditions (Pouysségur et al., 2006). HIF1α stabilization can be achieved also chemically by dimethyloxalylglycine (DMOG), which inhibits its degradation. Exposure of cells to DMOG stabilized HIF1α, which was accompanied by increased phosphorylation of

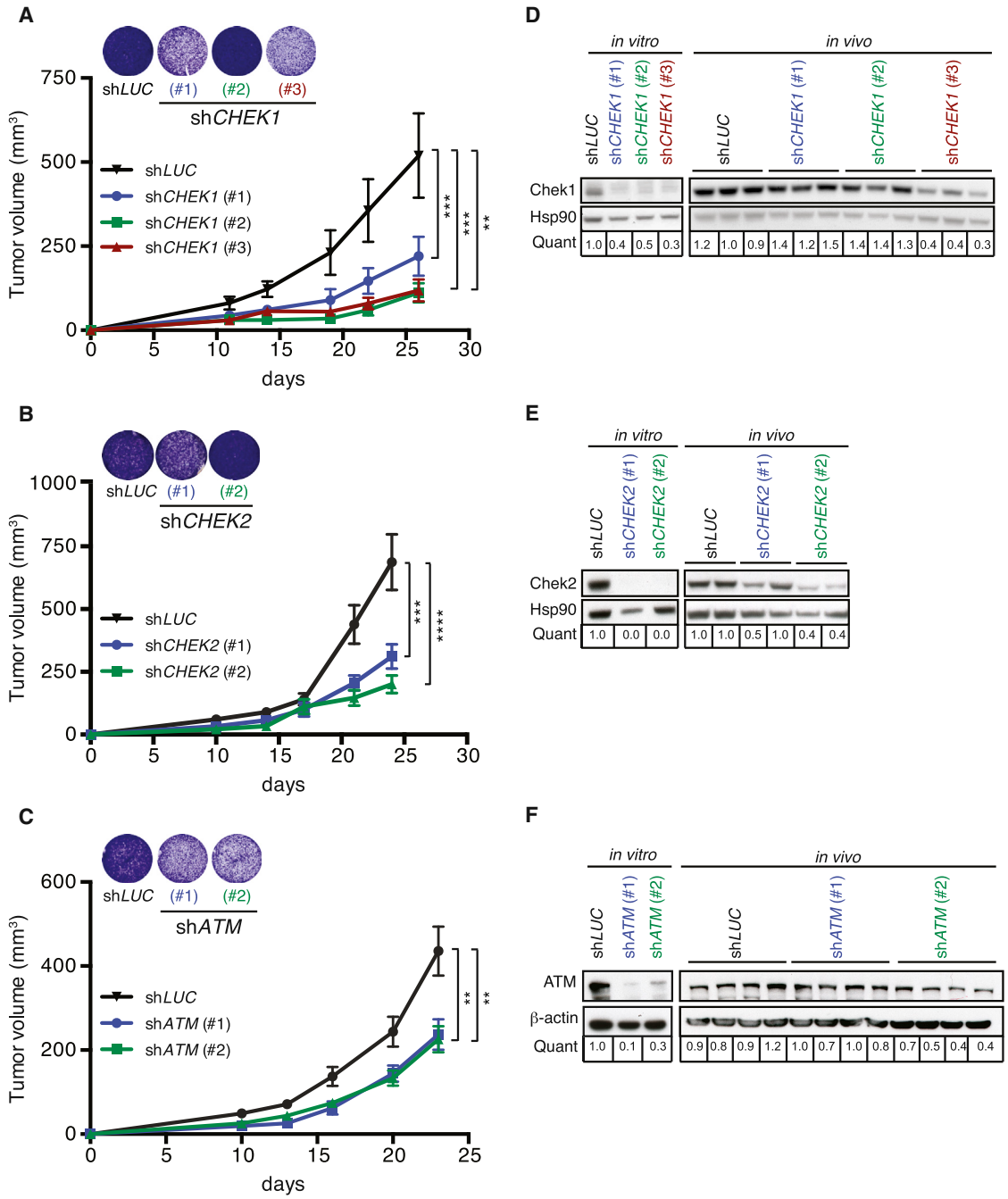

Figure 3. Critical Role for DNA Damage Response Factors during Melanoma Expansion

(A) Tumor growth of 888mel cells stably transduced with shRNAs targeting *CHEK1* or *LUC* and injected s.c. into both flanks of five NSG mice. **p = 0.006;***p = 0.0009. Data are presented as mean ± SEM. Inserts show stainings of transduced cells plated in equal numbers and grown in vitro for 8 days. See also Figures S3B and S3F.

(B) Tumor growth of 888mel cells stably transduced with shRNAs targeting *CHEK2* or *LUC* and injected s.c. into both flanks of NSG mice (five mice per group). ***p = 0.0009;****p < 0.00001. Data are presented as mean ± SEM. Inserts show stainings of transduced cells plated in equal numbers and grown in vitro for 8 days. See also Figures S3C and S3G.

(C) Tumor growth of 888mel cells stably transduced with shRNAs targeting *ATM* or *LUC* and injected s.c. into both flanks of NSG mice (five mice per group). **p < 0.007. Data are presented as mean ± SEM. Inserts show stainings of transduced cells plated in equal numbers and grown in vitro for 8 days. See also Figures S3D and S3H.

(D–F) Chek1, Chek2, and ATM expression was analyzed by western blotting before in vivo transplantation and in tumors at the end of the experiment. β-Actin and Hsp90 serve as loading controls. Densitometry measurements of bands were performed on each blot, and adjusted values relative to loading controls are shown bellow the respective bands (Quant).

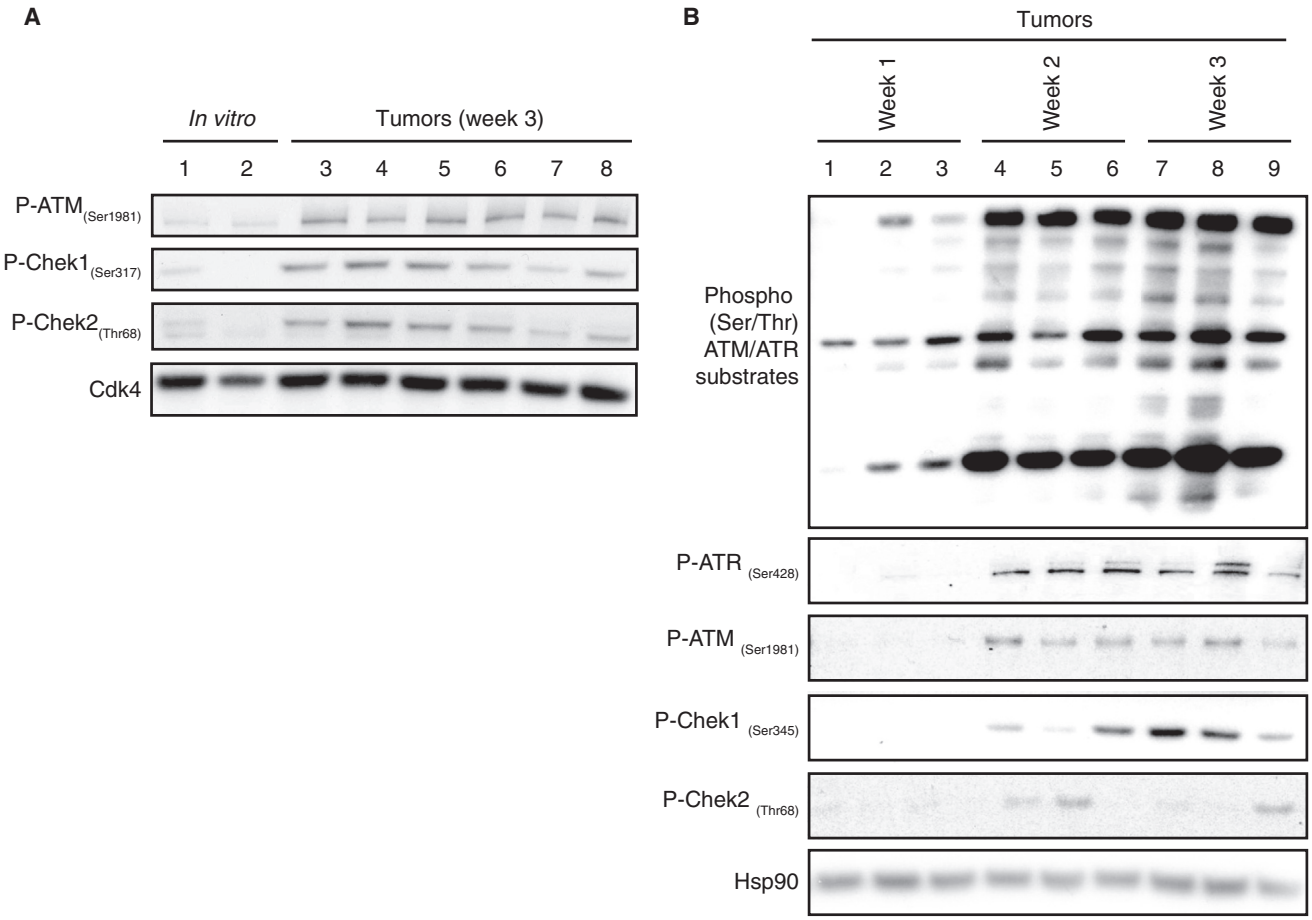

Figure 4. The DNA Response Pathway Is Activated during Tumor Expansion In Vivo

(A) Western blot analysis for DDR activation of 888mel cells grown in vitro versus 888mel tumors grown subcutaneously for 3 weeks in both flanks of three mice. (B) In vivo time course experiment. For each time point, two mice were s.c. injected with 888mel cells (both flanks) and tumors were harvested 1, 2, and 3 weeks after inoculation as indicated and analyzed by western blotting for activation of DDR factors. Hsp90 and Cdk4 serve as loading controls. See also Figure S4.

particularly Chek1 and Chek2, indicating that HIF1α can induce (at least these aspects of) DDR activation (Figure 5C).

To assess an in vivo correlation between hypoxia and DDR, we performed a series of immunohistochemical stainings of phospho-Chek2, phospho-ATM/ATR substrates and γH2AX on xenografted tumors (Figure 5D). This analysis revealed that the hypoxic areas in the tumors, as illustrated by the hematoxylin and eosin (H&E) staining showing many pyknotic/necrotic cells (see inset) and highlighted by the staining of pimonidazole, corresponded to the DDR areas as indicated by the intense staining of phospho-ATM/ATR substrates and γH2AX. Although few cells were positive for phospho-Chek2 staining, the positive cells were distinguishably localized in the areas where other DDR proteins were highly expressed. Furthermore, melanoma cells showed high Ki67 expression throughout the entire tumor.

HIF Stabilization Sensitizes Melanoma Cells to Chek1/2 Inhibition In Vitro

Since melanoma cells under hypoxic conditions and with induced levels of HIF1α exhibited increased DDR, we hypothesized that they may be more sensitive to the effects of pharmacologic Chek1/2 inhibition. Exposure to either AZD7762, an inhibitor that blocks Chek1/2 activity (Figure S5A), or DMOG caused little melanoma cell death in vitro. In contrast, combination of these compounds caused massive melanoma cell death, as illustrated by PARP cleavage and cell viability assays for several melanoma cell lines (including 888mel in which the screen was performed; Figures 6A and 6B). Of note, this effect appeared to be shared by *BRAF* and *NRAS* mutant melanomas and independent of *TP53* mutational status or activity (Figure S5B; Table S1). The effect of DMOG was dependent on HIF signaling, since depletion of *ARNT* (encoding HIF1β, the essential partner of HIF1α) protected DMOG-treated cells from death upon Chek1/2 inhibition (Figures 6C, S5C, and S5D).

Because the emergence of resistance to BRAF inhibition poses a major clinical challenge, we also determined the sensitivity to Chek1/2 inhibition in combination with DMOG in two sets of matched treatment-naive and BRAF-inhibitor-resistant cell lines. The resistant cell lines were as sensitive to the combination treatment as their parental counterparts (Figure 6D). To determine whether this could be recapitulated in a clinically more relevant

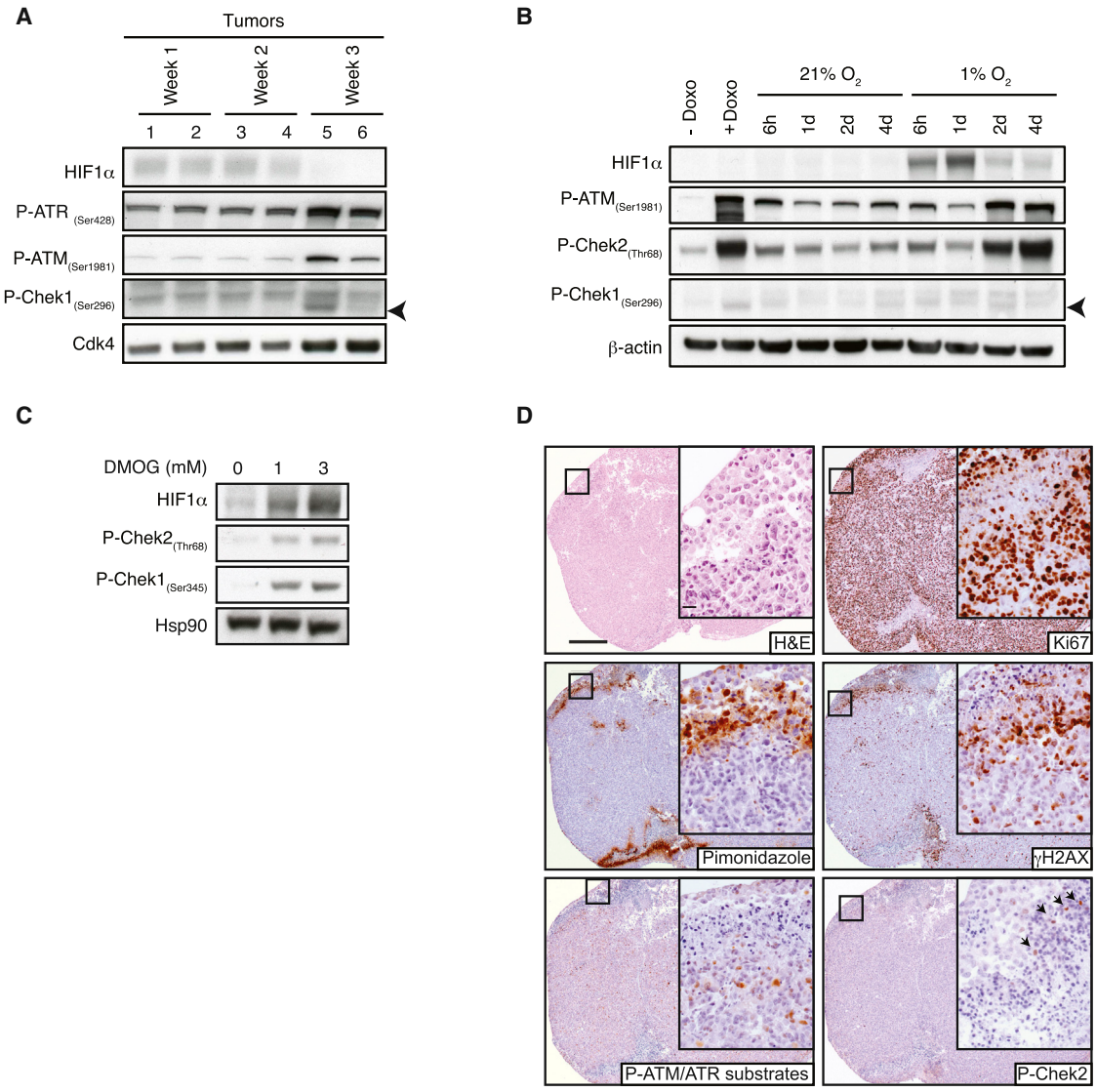

Figure 5. DDR Signaling Is Induced by Hypoxia and HIF1α Signaling In Vitro and Colocalizes with Hypoxic Areas of Tumors In Vivo

(A) In vivo time course experiment. For each time point, two mice were s.c. injected with 888mel cells (both flanks) and tumors were harvested 1, 2, and 3 weeks after inoculation and analyzed for HIF1α expression and DDR activation. Two tumors were analyzed per time point. Arrowhead points at phospho-Chek1. Cdk4 serves as loading control.

(B) 888mel cells were cultured under regular in vitro conditions (21% O_2) or reduced oxygen tension (1% O_2) for different periods of time as indicated. Doxorubicin (Doxo) treatment serves as a positive control for phosphorylation of DDR proteins. Arrowhead points at phospho-Chek1. β-Actin serves as loading control.

(C) 888mel cells were treated with different concentrations of DMOG for 1 day and analyzed for phosphorylation of Chek 1 and 2. Hsp90 serves as loading control.

(D) Microphotographs of H&E and pimonidazole stainings as well as immunohistochemistry of γH2AX, phospho-Chek2, phospho-ATM/ATR substrates, and Ki67 of a representative xenografted tumor harvested 1 week after s.c. injection. The hypoxic areas in the tumor are the areas with many pyknotic/apoptotic cells as illustrated by H&E stainings, which are highlighted by pimonidazole stainings. The same areas are strongly positive for γH2AX and, to a lesser extent, phospho-ATM/ATR substrates. Although very few cells are positive for phospho-Chek2, the positive ones are restricted to the hypoxic areas. Tumors cells are generally positive for Ki67 throughout the entire tumor. Squares indicate insets. Scale bars represent 500 μm (2.5×) and 20 μm (40×, insets).

setting, we established low-passage cell lines from patient-derived xenografts (PDX; M026) of a melanoma patient prior to therapy and after resistance to vemurafenib treatment had occurred (Figure S5E). Again, we observed a strong combinatorial effect also for the resistant cells, suggesting a broad effectiveness of this antitumor strategy in melanoma (Figure 6D).

Hypoxia Enhances Tumor Killing by Pharmacological Chek1/2 Inhibition In Vivo

The results shown above raise the possibility that reduced oxygen conditions render melanoma cells more vulnerable to inhibition of the DDR, providing a rationale for pharmacological modulation of both of these factors in vivo. To explore this

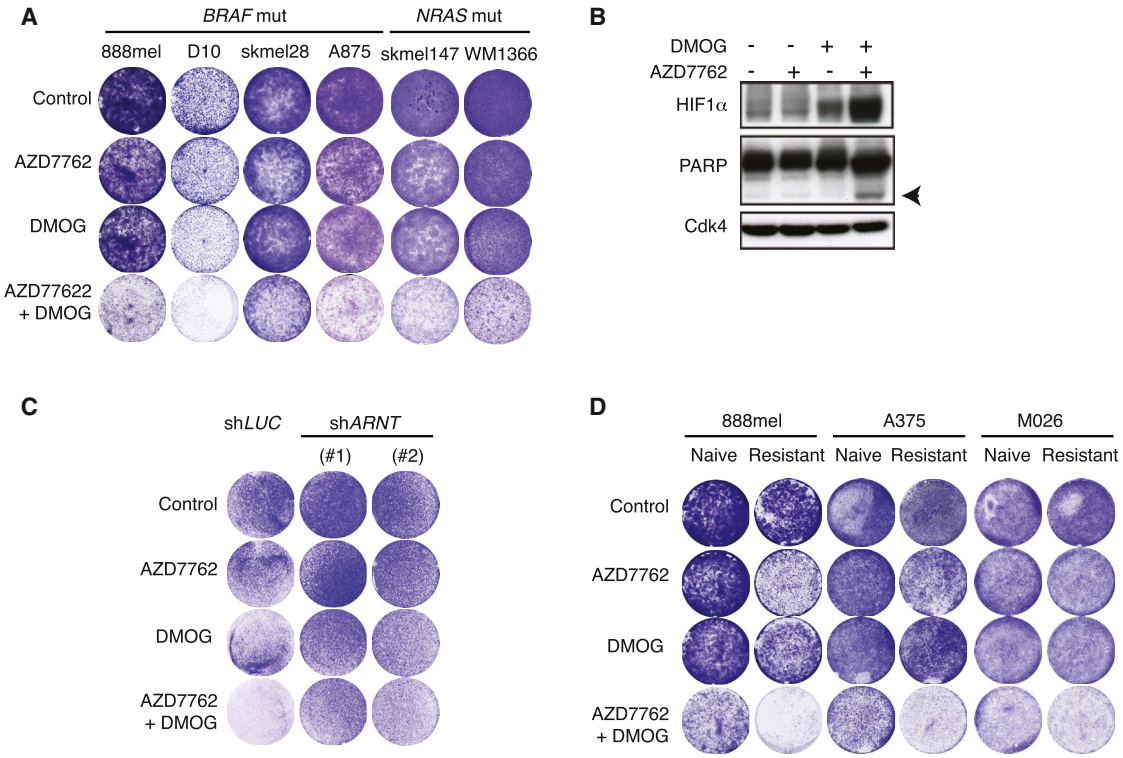

Figure 6. HIF Stabilization Sensitizes Melanoma Cells to Chek1/2 Inhibition In Vitro

(A) 888mel, D10, skmel28, A875, skmel147, and WM1366 human melanoma cell lines were plated in equal numbers and exposed to AZD7762 (80 nM for 888mel; 600 nM for D10; 160 nM for skmel28 and A875, 10 nM for skmel147 and 15 nM for WM1366), DMOG (1 mM for 888mel and skmel28; 1.5 mM for D10 and A875; 0.25mM for skmel147 and 0.75mM for WM1366) either alone or in combination as indicated. Plates were stained after 6 days.

(B) 888mel cells were treated with AZD7762 (80 nM), DMOG (1 mM), or the combination for 6 days. Cell lysates were analyzed by western blotting for the indicated antibodies. Arrowhead points at cleaved PARP. Cdk4 serves as a loading control.

(C) 888mel cells carrying either sh*LUC* or sh*ARNT* were plated at equal numbers and exposed to AZD7762 (80 nM), DMOG (1 mM), or the combination. Plates were stained after 6 days. See also Figures S5C and S5D.

(D) BRAF-inhibitor-naive and BRAF-inhibitor-resistant cell line pairs were treated with AZD7762 (80 nM for 888mel and 888melR, A375 and A375R; 20 nM for M026 and M026R.X1), DMOG (1 mM for 888mel and M026.X1 pairs and 1.5 mM for A375 pair), or the combination for 6 days. M026 refers to a melanoma patient from whom PDX-derived cell lines were generated prior to treatment ("Naive") and after relapse ("Resistant"). See also Figure S5E.

possibility, we first used the AZD7762 compound to treat mice immediately after transplantation of human melanoma cells. This single agent treatment significantly delayed tumor outgrowth, again illustrating the in vitro/in vivo window seen in the screens (Figure S6A). Systemic drug toxicity was not observed. Control tumors had large necrotic areas that were largely confined to the inner tumor mass, indicative of insufficient oxygen supply. Although AZD7762-treated tumors were smaller, they were much more necrotic and these areas extended well beyond the tumor centers (Figure S6B). Of more clinical relevance, a similar extent of tumor suppression was achieved upon treatment after tumors had already established (Figure 7A), excluding that the effect seen after Chek1/2 inhibition was simply due to a consequence of impairment of early tumor cell engraftment.

Above, we showed that a low-passage PDX-derived cell line from a melanoma patient with acquired resistance to vemurafenib could be effectively eliminated by Chek1/2 inhibition in combination with DMOG. Next, we determined the treatment response of a PDX from a patient with primary resistance to vemurafenib (Figure S6C). Chek1/2 inhibition after establishment of the xenograft strongly delayed tumor growth (Figure 7B).

Finally, we set out to recapitulate in vivo the cooperative induction of tumor cell death upon hypoxia and DDR inhibition that we had observed in vitro. Treatment of transplanted melanoma cells with the monoclonal antibody bevacizumab, which neutralizes VEGF, accelerated the appearance of large hypoxic areas surrounding necrotic tumor fields after 1 week of tumor transplantation (Figure 7C). More importantly, when bevacizumab and AZD7762 were used in combination, synergistic tumor inhibition was achieved (Figures 7D and S6D). Similarly, synthetic lethality by hypoxia induction and Chek1/2 inhibition in vivo was observed for the PDX derived from a melanoma patient who had acquired resistance to BRAF inhibition ("M026R.X2"; Figure 7E). We conclude from these results that the combined inhibition of DDR kinases and induction of hypoxia represents a potentially valuable treatment option for melanoma, inclusively in the context of BRAF-inhibitor-resistant tumor cells.

DISCUSSION

This study aimed to identify pharmacologically tractable cancer targets by building on a fundamental principle: non-oncogene addiction in vivo. We reasoned that physiologic experimental conditions could identify critical cancer vulnerabilities that would not readily be discovered in cells cultured in vitro. Indeed, in vivo negative-selection screens can uncover specific dependencies (Beronja et al., 2013; Meacham et al., 2009; Possemato et al., 2011). For melanoma, single cells can drive tumor growth (Quintana et al., 2008, 2010). Here, by genetic barcoding, we demonstrate and exploit a related property, that is, that melanoma cells under such conditions contribute to tumor growth in a polyclonal fashion. It is particularly the latter property that enabled us to perform a negative-selection screen: had the tumors been formed in a (oligo)clonal fashion, most of the shRNA library would have been lost randomly.

The parallel in vitro and in vivo screens demonstrated a more profound requirement for DDR kinases for survival of melanoma cells when proliferating in mice than upon passaging in culture. We show that this is caused, at least in significant part, by increased HIF-mediated hypoxic signaling, which leads to DDR activation in vivo. Consistent with this, tumor cells are under selective pressure to manipulate their microenvironment by secreting soluble factors, including proangiogenic factors to counteract the lack of blood vessels (Pouysségur et al., 2006).

Recapitulating one critical aspect of these conditions in vitro, we show that hypoxia activates DDR signaling and sensitizes tumor cells to Chek1/2 inhibition. This is consistent with, and extends, previous data on the relationship between hypoxia and activation of the DDR pathway (Bencokova et al., 2009; Hammond et al., 2007; Olcina et al., 2010), which does not always require actual DNA damage (Hammond et al., 2007). Also, DNA replication stress has been shown to predispose melanoma cells to DDR inhibition (Brooks et al., 2013; Ferrao et al., 2011). We show that in vivo, tumor expansion coincides with activation of several DDR factors, particularly Chek1, Chek2, ATM, and ATR. Interestingly, this was accompanied by abundant activation of the histone H2AX, indicative of ATM/ATR-dependent DDR signaling. That this was preceded by HIF1α induction is in agreement with our finding that low oxygen levels trigger DDR activation in a HIF-dependent manner in vitro. Consistently, both HIF1α or HIF2α are highly expressed in melanoma and represent poor-prognosis biomarkers (Giatromanolaki et al., 2003; Keith et al., 2012). We show that preventing stabilization of both HIF isoforms by HIF1β depletion protected hypoxic tumor cells from the cytotoxic effect of Chek1/2 inhibition. This result suggests that the induction of HIF-dependent DDR can be exploited pharmacologically to cause melanoma cell death in vivo, which indeed we demonstrate here.

Our study suggests that while single-agent targeting of Chek1/2 may have a moderate therapeutic benefit, full exploitation of this dependency requires targeting of another signal, particularly one that contributes to DDR activation. We show here that this second signal may be angiogenic blockage and, consequently, the (pharmacological) induction of hypoxia. This model of combinatorial therapy is consistent with ongoing exploration on the targeting of Chek1/2 in the context of DNA-directed chemotherapy and radiotherapy (Landau et al., 2012; Ma et al., 2011, 2012, 2013; Morgan et al., 2010; Sausville et al., 2014; Syljuåsen et al., 2006). Because we found evidence implicating both ATM/Chek2 and ATR/Chek1 in response to hypoxia, and given the crosstalk between these signaling routes (Curtin, 2012), we reasoned that pharmacological targeting of both checkpoint kinases would be more successful under hypoxic conditions.

It is noteworthy that Chek1/2 inhibition eliminated both BRAF-inhibitor-sensitive and BRAF-inhibitor-resistant cells, which is important given the common resistance of *BRAF* mutant melanomas to targeted therapy. We also show that an antiangiogenic drug, such as bevacizumab, is a new in vivo synthetic lethal partner of DDR inhibition in melanomas. It is conceivable that this combinatorial therapeutic strategy will also be effective in other tumor types, such as breast and pancreatic cancers (in which Chek1/2 inhibition is being explored), but this remains to be determined.

In conclusion, we show that during melanoma expansion, the DDR signaling pathway becomes essential in dealing with the limited oxygen supply. Additional factors, including nutrients and glucose deprivation, may contribute to the stress conditions that tumors face as well. A limitation of xenotransplantation of human tumor cells in immunodeficient mice is the absence of immune cells, which play an important role in tumor behavior. This notwithstanding, by demonstrating that pharmacologically induced hypoxia synergizes with DDR inhibitors to cause melanoma cell death, our results highlight the advantage of an in vivo screening approach. Thus, an in vivo negative-selection approach can be used to identify specific synthetic lethal relationships that may be explored clinically.

EXPERIMENTAL PROCEDURES

In Vivo and In Vitro Screens

To examine the feasibility of negative-selection in vivo screens, a barcode screen was performed as described in Supplemental Experimental Procedures. For shRNA screens, a lentivirus-based kinome shRNA library (four pools) was used to transduce 888mel cells (MOI < 0.2). After puromycin selection (1 μg/ml), two reference samples were collected as controls. Next, tumor cells (5×10^5 per injection) were either injected s.c. into six NSG mice or plated into six independent plates (5×10^5) for in vitro culture. Tumors were removed from the mice and cultured cells were harvested, and genomic DNA was used to recover shRNAs by PCR amplification followed by deep sequencing. Three analyses were performed independently in parallel: (1) tumors versus cultured cells ($\log_2$ fold change < -1); (2) tumors versus references ($\log_2$ fold change < -2.5), and (3) cultured cells versus references ($\log_2$ fold change < -2.5). Genes targeted with at least two shRNAs in each of the analysis were considered hits with an enhanced in vivo effect. A more detailed protocol is described in Supplemental Experimental Procedures.

In Vitro Experiments

All cell lines were cultured in Dulbecco's modified Eagle's medium supplemented with 9% fetal bovine serum (Sigma), 2 mM glutamine, 100 U/ml penicillin, and 0.1 mg/ml streptomycin (all Gibco). For knockdown experiments, shRNA (from TRC-Hs1.0; see sequence details in the Supplemental Experimental Procedures) were transfected into HEK293T cells and the lentivirus-containing supernatant was used to transduce 888mel cells, followed by puromycin selection. To generate BRAF-inhibitor-resistant cell lines, 888mel and A375 cells were exposed to increasing concentrations of PLX4720 (Selleck; up to 3 μM). Cell viability was measured by either crystal violet staining or CellTiter-Blue (Promega) and fluorescence determined with an Infinite M200

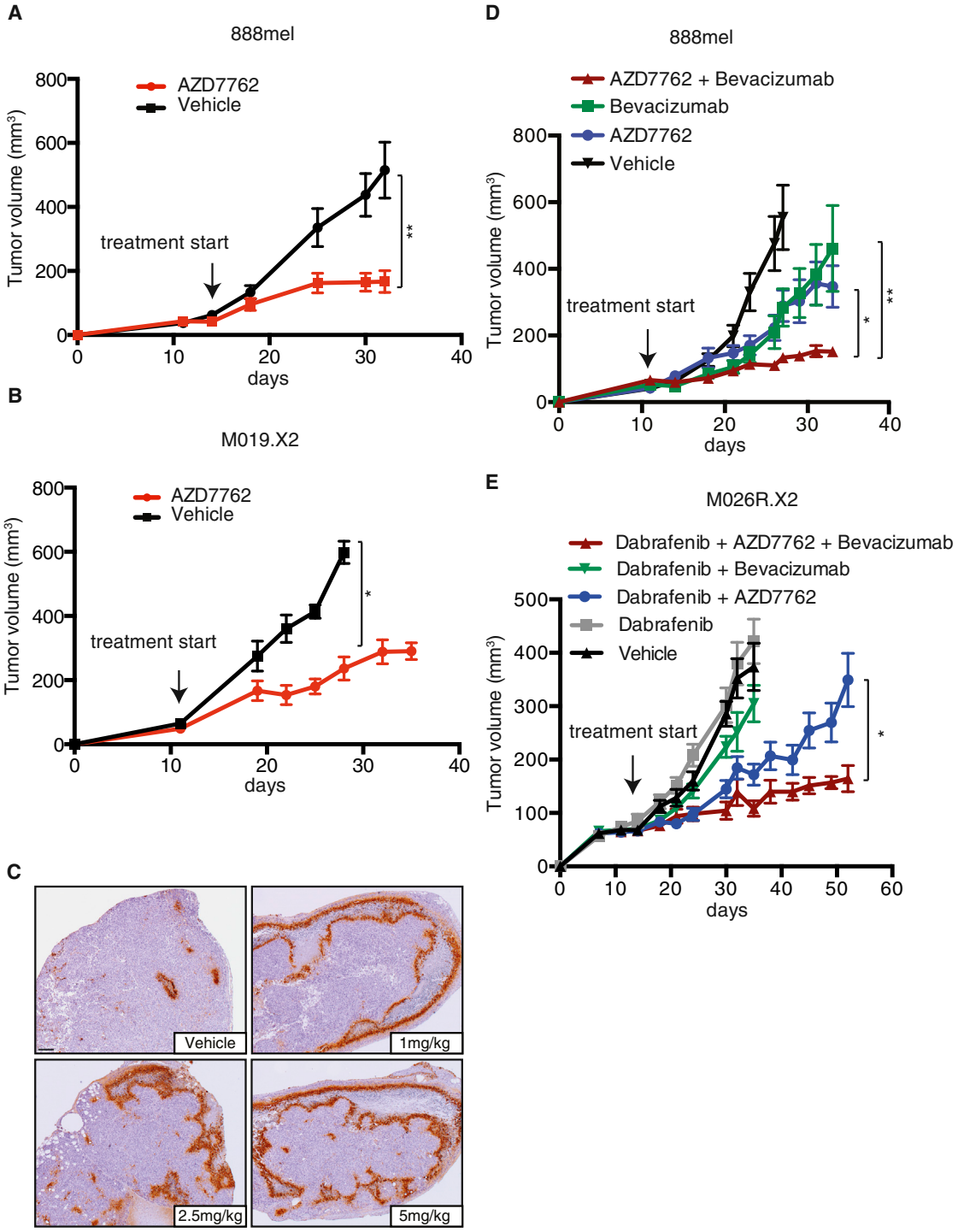

Figure 7. Hypoxia Enhances Tumor Killing by Pharmacological Chek1/2 Inhibition In Vivo

(A) NSG mice were transplanted with 888mel cells (five animals per group, both flanks) and treated with 2 mg/kg AZD7762 (red line) or with vehicle control (black line) starting after tumors had reached approximately 50 mm^3. **$p < 0.007$. Data are presented as mean ± SEM.

(B) NSG mice were transplanted with M019.X2 cells (five animals per group, both flanks) and treated with 2 mg/kg AZD7762 (red line) or with vehicle control (black line) after tumors had reached approximately 50 mm^3. *$p < 0.02$. Data are presented as mean ± SEM.

(C) NSG mice were transplanted with 888mel cells and treated with vehicle or 1, 2.5, or 5 mg/kg bevacizumab for 7 days (five animals per group, both flanks). Hypoxic tumor regions are indicated by immunohistochemical detection of pimonidazole in 888mel xenografts. Scale bar represents 200 μm (5×).

(legend continued on next page)

microplate reader (Tecan). AZD7762 (Selleck), DMOG (Frontier Scientific), and cisplatin (Accord) were used as described in the text.

In Vivo Experiments

Human melanoma cell lines were embedded in Matrigel 1:1 in medium and s.c. injected into NSG mice (5×10^5 per injection). A more detailed protocol on patient-derived xenografts is described in Supplemental Experimental Procedures. Tumor growth was measured and calculated by the formula $(a*b^2)/2$, with a being the longest diameter and b the perpendicular diameter. AZD7762 (Selleck) (2–2.5 mg/kg) was dissolved in 11.3% 2-hydroxypropyl-β-cyclodextrin (HPβCD) in 0.9% NaCl (pH 4) and administered intraperitoneally (i.p.) three times a week. Bevacizumab (Roche) (1–5 mg/kg) was diluted in 0.9% NaCl and administered i.p. twice weekly. Dabrafenib (Abmole) (30 mg/kg) was dissolved in 0.5% hydroxypropyl methylcellulose (HPMC), 0.2% Tween80 and administered orally 6 days a week. Animals were sacrificed by cervical dislocation or CO_2, and tumor volume and weight were measured. To assess tumor hypoxia, mice were injected i.p. with 1.5 mg/kg pimonidazole (Hypoxyprobe) in 0.9% NaCl 1 hr prior to sacrifice. Statistical analyses were done with two-tailed t tests for two experimental group comparisons and one-way ANOVA corrected for multiple comparisons (Holm-Sidak) when more than two experimental groups were analyzed (Prism; GraphPad Software). Tumor volumes and weights at the experimental endpoints were used for analyses. Animal experiments were performed following local and international regulations and ethical guidelines and have been authorized by the local experimental animal committee at The Netherlands Cancer Institute.

ACCESSION NUMBERS

Relevant data sets have been made available through the NCBI Gene Expression Omnibus (http://www.ncbi.nlm.nih.gov/geo) with the accession number GSE61826.

SUPPLEMENTAL INFORMATION

Supplemental Information includes Supplemental Experimental Procedures, six figures, and one table and can be found with this article online at http://dx.doi.org/10.1016/j.celrep.2014.10.024.

AUTHOR CONTRIBUTIONS

P.A.P and D.S.P. conceived the project, designed and analyzed the experiments, and wrote the manuscript. P.A.P performed most experiments. J.M. designed, performed, and analyzed validation experiments. C.G. and T.N.S. helped design and perform the barcode screen. J.C.N.K. performed validation experiments. K.K. and A.S. set up the PDX platform. A.S. helped with animal experiments and generation of cell lines. O.K. analyzed exome-sequencing data. J.Y.S. performed pathological analysis of tumors. C.L., B.G., M.M., and R.L.B. analyzed the screen data. X.H. and M.A.S. helped with screen analysis and validation experiments. L.W. provided input into designing the barcode screen. All authors discussed the results and commented on the manuscript.

ACKNOWLEDGMENTS

We thank Adrian Begg, Michael Hauptmann, Hein te Riele, Naoki Uno, Rodrigo Leite de Oliveira, Christian Blank, and John Haanen for critical discussions, Margareth Morgan for advice on AZD7762, and all members of the Peeper laboratory for their valuable input. This work was financially supported by a grant from the Dutch Cancer Society (NKI-2013-5799) to K.K. and D.S.P. and a Queen Wilhelmina award and ERC Synergy grant "COMBATCANCER" to D.S.P.

Received: January 31, 2014
Revised: August 12, 2014
Accepted: October 10, 2014
Published: November 6, 2014

REFERENCES

Bencokova, Z., Kaufmann, M.R., Pires, I.M., Lecane, P.S., Giaccia, A.J., and Hammond, E.M. (2009). ATM activation and signaling under hypoxic conditions. Mol. Cell. Biol. *29*, 526–537.

Beronja, S., Janki, P., Heller, E., Lien, W.-H., Keyes, B.E., Oshimori, N., and Fuchs, E. (2013). RNAi screens in mice identify physiological regulators of oncogenic growth. Nature *501*, 185–190.

Boiko, A.D., Razorenova, O.V., van de Rijn, M., Swetter, S.M., Johnson, D.L., Ly, D.P., Butler, P.D., Yang, G.P., Joshua, B., Kaplan, M.J., et al. (2010). Human melanoma-initiating cells express neural crest nerve growth factor receptor CD271. Nature *466*, 133–137.

Brooks, K., Oakes, V., Edwards, B., Ranall, M., Leo, P., Pavey, S., Pinder, A., Beamish, H., Mukhopadhyay, P., Lambie, D., and Gabrielli, B. (2013). A potent Chk1 inhibitor is selectively cytotoxic in melanomas with high levels of replicative stress. Oncogene *32*, 788–796.

Chapman, P.B., Hauschild, A., Robert, C., Haanen, J.B., Ascierto, P., Larkin, J., Dummer, R., Garbe, C., Testori, A., Maio, M., et al.; BRIM-3 Study Group (2011). Improved survival with vemurafenib in melanoma with BRAF V600E mutation. N. Engl. J. Med. *364*, 2507–2516.

Curtin, N.J. (2012). DNA repair dysregulation from cancer driver to therapeutic target. Nat. Rev. Cancer *12*, 801–817.

Davies, H., Bignell, G.R., Cox, C., Stephens, P., Edkins, S., Clegg, S., Teague, J., Woffendin, H., Garnett, M.J., Bottomley, W., et al. (2002). Mutations of the BRAF gene in human cancer. Nature *417*, 949–954.

Farmer, H., McCabe, N., Lord, C.J., Tutt, A.N.J., Johnson, D.A., Richardson, T.B., Santarosa, M., Dillon, K.J., Hickson, I., Knights, C., et al. (2005). Targeting the DNA repair defect in BRCA mutant cells as a therapeutic strategy. Nature *434*, 917–921.

Ferrao, P.T., Bukczynska, E.P., Johnstone, R.W., and McArthur, G.A. (2011). Efficacy of CHK inhibitors as single agents in MYC-driven lymphoma cells. Oncogene *31*, 1661–1672.

Flaherty, K.T., Robert, C., Hersey, P., Nathan, P., Garbe, C., Milhem, M., Demidov, L.V., Hassel, J.C., Rutkowski, P., Mohr, P., et al.; METRIC Study Group (2012). Improved survival with MEK inhibition in BRAF-mutated melanoma. N. Engl. J. Med. *367*, 107–114.

Gerlach, C., Rohr, J.C., Perié, L., van Rooij, N., van Heijst, J.W.J., Velds, A., Urbanus, J., Naik, S.H., Jacobs, H., Beltman, J.B., et al. (2013). Heterogeneous differentiation patterns of individual CD8+ T cells. Science *340*, 635–639.

Giatromanolaki, A., Sivridis, E., Kouskoukis, C., Gatter, K.C., Harris, A.L., and Koukourakis, M.I. (2003). Hypoxia-inducible factors 1alpha and 2alpha are related to vascular endothelial growth factor expression and a poorer

(D) NSG mice were transplanted with 888mel cells (five animals per group, both flanks) and treated with vehicle, 2.5 mg/kg AZD7762, 1 mg/kg bevacizumab, or the combination. Treatment started after tumors had reached approximately 50 mm^3. Vehicle-treated mice were sacrificed at day 27 when they reached the maximum tumor volume according to local and international regulations. The remaining animals were maintained under treatment until day 33. *p = 0.04 (for both AZD7762 and bevacizumab single treatments); **p = 0.006. Data are presented as mean ± SEM.

(E) M026R.X1 tumors were dissociated and transplanted s.c. into NSG mice (five animals per group, both flanks). All mice received dabrafenib (30 mg/kg) continuously starting 1 day after transplantation. Treatment with vehicle, 2.5 mg/kg AZD7762, 1 mg/kg bevacizumab, or the combination started after tumors (now referred to as M026R.X2) had reached approximately 50 mm^3. Treated mice were sacrificed at day 33. AZD7762- and combination-treated animals were maintained on treatment until day 54. *p < 0.05. Data are presented as mean ± SEM.

prognosis in nodular malignant melanomas of the skin. Melanoma Res. *13*, 493–501.

Hammond, E.M., Kaufmann, M.R., and Giaccia, A.J. (2007). Oxygen sensing and the DNA-damage response. Curr. Opin. Cell Biol. *19*, 680–684.

Hauschild, A., Grob, J.-J., Demidov, L.V., Jouary, T., Gutzmer, R., Millward, M., Rutkowski, P., Blank, C.U., Miller, W.H., Jr., Kaempgen, E., et al. (2012). Dabrafenib in BRAF-mutated metastatic melanoma: a multicentre, open-label, phase 3 randomised controlled trial. Lancet *380*, 358–365.

Hingorani, S.R., Jacobetz, M.A., Robertson, G.P., Herlyn, M., and Tuveson, D.A. (2003). Suppression of BRAF(V599E) in human melanoma abrogates transformation. Cancer Res. *63*, 5198–5202.

Jang, S., and Atkins, M.B. (2013). Which drug, and when, for patients with BRAF-mutant melanoma? Lancet Oncol. *14*, e60–e69.

Kaelin, W.G., Jr. (2004). Gleevec: prototype or outlier? Sci. STKE *2004*, pe12.

Kaelin, W.G., Jr. (2005). The concept of synthetic lethality in the context of anticancer therapy. Nat. Rev. Cancer *5*, 689–698.

Kaplon, J., Zheng, L., Meissl, K., Chaneton, B., Selivanov, V.A., Mackay, G., van der Burg, S.H., Verdegaal, E.M.E., Cascante, M., Shlomi, T., et al. (2013). A key role for mitochondrial gatekeeper pyruvate dehydrogenase in oncogene-induced senescence. Nature *498*, 109–112.

Karbowniczek, M., Spittle, C.S., Morrison, T., Wu, H., and Henske, E.P. (2008). mTOR is activated in the majority of malignant melanomas. J. Invest. Dermatol. *128*, 980–987.

Keith, B., Johnson, R.S., and Simon, M.C. (2012). HIF1α and HIF2α: sibling rivalry in hypoxic tumour growth and progression. Nat. Rev. Cancer *12*, 9–22.

Landau, H.J., McNeely, S.C., Nair, J.S., Comenzo, R.L., Asai, T., Friedman, H., Jhanwar, S.C., Nimer, S.D., and Schwartz, G.K. (2012). The checkpoint kinase inhibitor AZD7762 potentiates chemotherapy-induced apoptosis of p53-mutated multiple myeloma cells. Mol. Cancer Ther. *11*, 1781–1788.

Lee, J.T., and Herlyn, M. (2007). Microenvironmental influences in melanoma progression. J. Cell. Biochem. *101*, 862–872.

Luo, J., Solimini, N.L., and Elledge, S.J. (2009). Principles of cancer therapy: oncogene and non-oncogene addiction. Cell *136*, 823–837.

Ma, C.X., Janetka, J.W., and Piwnica-Worms, H. (2011). Death by releasing the breaks: CHK1 inhibitors as cancer therapeutics. Trends Mol. Med. *17*, 88–96.

Ma, C.X., Cai, S., Li, S., Ryan, C.E., Guo, Z., Schaiff, W.T., Lin, L., Hoog, J., Goiffon, R.J., Prat, A., et al. (2012). Targeting Chk1 in p53-deficient triple-negative breast cancer is therapeutically beneficial in human-in-mouse tumor models. J. Clin. Invest. *122*, 1541–1552.

Ma, C.X., Ellis, M.J.C., Petroni, G.R., Guo, Z., Cai, S.-R., Ryan, C.E., Craig Lockhart, A., Naughton, M.J., Pluard, T.J., Brenin, C.M., et al. (2013). A phase II study of UCN-01 in combination with irinotecan in patients with metastatic triple negative breast cancer. Breast Cancer Res. Treat. *137*, 483–492.

Meacham, C.E., Ho, E.E., Dubrovsky, E., Gertler, F.B., and Hemann, M.T. (2009). In vivo RNAi screening identifies regulators of actin dynamics as key determinants of lymphoma progression. Nat. Genet. *41*, 1133–1137.

Morgan, M.A., Parsels, L.A., Zhao, L., Parsels, J.D., Davis, M.A., Hassan, M.C., Arumugarajah, S., Hylander-Gans, L., Morosini, D., Simeone, D.M., et al. (2010). Mechanism of radiosensitization by the Chk1/2 inhibitor AZD7762 involves abrogation of the G2 checkpoint and inhibition of homologous recombinational DNA repair. Cancer Res. *70*, 4972–4981.

Morris, E.J., Jha, S., Restaino, C.R., Dayananth, P., Zhu, H., Cooper, A., Carr, D., Deng, Y., Jin, W., Black, S., et al. (2013). Discovery of a novel ERK inhibitor with activity in models of acquired resistance to BRAF and MEK inhibitors. Cancer Discov. *3*, 742–750.

Olcina, M., Lecane, P.S., and Hammond, E.M. (2010). Targeting hypoxic cells through the DNA damage response. Clin. Cancer Res. *16*, 5624–5629.

Possemato, R., Marks, K.M., Shaul, Y.D., Pacold, M.E., Kim, D., Birsoy, K., Sethumadhavan, S., Woo, H.-K., Jang, H.G., Jha, A.K., et al. (2011). Functional genomics reveal that the serine synthesis pathway is essential in breast cancer. Nature *476*, 346–350.

Pouysségur, J., Dayan, F., and Mazure, N.M. (2006). Hypoxia signalling in cancer and approaches to enforce tumour regression. Nature *441*, 437–443.

Quintana, E., Shackleton, M., Sabel, M.S., Fullen, D.R., Johnson, T.M., and Morrison, S.J. (2008). Efficient tumour formation by single human melanoma cells. Nature *456*, 593–598.

Quintana, E., Shackleton, M., Foster, H.R., Fullen, D.R., Sabel, M.S., Johnson, T.M., and Morrison, S.J. (2010). Phenotypic heterogeneity among tumorigenic melanoma cells from patients that is reversible and not hierarchically organized. Cancer Cell *18*, 510–523.

Roesch, A., Fukunaga-Kalabis, M., Schmidt, E.C., Zabierowski, S.E., Brafford, P.A., Vultur, A., Basu, D., Gimotty, P., Vogt, T., and Herlyn, M. (2010). A temporarily distinct subpopulation of slow-cycling melanoma cells is required for continuous tumor growth. Cell *141*, 583–594.

Sausville, E., Lorusso, P., Carducci, M., Carter, J., Quinn, M.F., Malburg, L., Azad, N., Cosgrove, D., Knight, R., Barker, P., et al. (2014). Phase I dose-escalation study of AZD7762, a checkpoint kinase inhibitor, in combination with gemcitabine in US patients with advanced solid tumors. Cancer Chemother. Pharmacol. *73*, 539–549.

Sawyers, C.L. (2005). Making progress through molecular attacks on cancer. Cold Spring Harb. Symp. Quant. Biol. *70*, 479–482.

Schatton, T., Murphy, G.F., Frank, N.Y., Yamaura, K., Waaga-Gasser, A.M., Gasser, M., Zhan, Q., Jordan, S., Duncan, L.M., Weishaupt, C., et al. (2008). Identification of cells initiating human melanomas. Nature *451*, 345–349.

Schepers, K., Swart, E., van Heijst, J.W.J., Gerlach, C., Castrucci, M., Sie, D., Heimerikx, M., Velds, A., Kerkhoven, R.M., Arens, R., and Schumacher, T.N. (2008). Dissecting T cell lineage relationships by cellular barcoding. J. Exp. Med. *205*, 2309–2318.

Shackleton, M., Quintana, E., Fearon, E.R., and Morrison, S.J. (2009). Heterogeneity in cancer: cancer stem cells versus clonal evolution. Cell *138*, 822–829.

Sharma, S.V., and Settleman, J. (2010). Exploiting the balance between life and death: targeted cancer therapy and "oncogenic shock". Biochem. Pharmacol. *80*, 666–673.

Solit, D.B., Garraway, L.A., Pratilas, C.A., Sawai, A., Getz, G., Basso, A., Ye, Q., Lobo, J.M., She, Y., Osman, I., et al. (2006). BRAF mutation predicts sensitivity to MEK inhibition. Nature *439*, 358–362.

Syljuåsen, R.G., Jensen, S., Bartek, J., and Lukas, J. (2006). Adaptation to the ionizing radiation-induced G2 checkpoint occurs in human cells and depends on checkpoint kinase 1 and Polo-like kinase 1 kinases. Cancer Res. *66*, 10253–10257.

Tsai, J., Lee, J.T., Wang, W., Zhang, J., Cho, H., Mamo, S., Bremer, R., Gillette, S., Kong, J., Haass, N.K., et al. (2008). Discovery of a selective inhibitor of oncogenic B-Raf kinase with potent antimelanoma activity. Proc. Natl. Acad. Sci. USA *105*, 3041–3046.